

Modulation Instability Induced Frequency Comb Generation in a Continuously Pumped Optical Parametric Oscillator

S. Mosca,^{1,*} M. Parisi,¹ I. Ricciardi,^{1,2} F. Leo,³ T. Hansson,⁴ M. Erkintalo,⁵ P. Maddaloni,^{1,2} P. De Natale,⁶ S. Wabnitz,^{7,8} and M. De Rosa^{1,2,†}

¹*CNR-INO, Istituto Nazionale di Ottica, Via Campi Flegrei 34, I-80078 Pozzuoli (NA), Italy*

²*INFN, Istituto Nazionale di Fisica Nucleare, Sez. di Napoli, Complesso Universitario di M.S. Angelo, Via Cintia, Napoli 80126, Italy*

³*OPERA-photonics, Université Libre de Bruxelles, 50 Avenue F. D. Roosevelt, CP 194/5, B-1050 Bruxelles, Belgium*

⁴*Dipartimento di Ingegneria dell'Informazione, Università di Brescia, Via Branze 38, I-25123 Brescia, Italy*

⁵*The Dodd-Walls Centre for Photonic and Quantum Technologies, Department of Physics, The University of Auckland, Auckland 1142, New Zealand*

⁶*CNR-INO, Istituto Nazionale di Ottica, Largo E. Fermi 6, I-50125 Firenze, Italy*

⁷*Dipartimento di Ingegneria dell'Informazione, Università di Brescia, and CNR-INO, Via Branze 38, I-25123 Brescia, Italy*

⁸*Novosibirsk State University, 1 Pirogova Street, Novosibirsk 630090, Russia*



(Received 28 March 2018; published 30 August 2018)

Continuously pumped passive nonlinear cavities can be harnessed for the creation of novel optical frequency combs. While most research has focused on third-order “Kerr” nonlinear interactions, recent studies have shown that frequency comb formation can also occur via second-order nonlinear effects. Here, we report on the formation of quadratic combs in optical parametric oscillator (OPO) configurations. Specifically, we demonstrate that optical frequency combs can be generated in the parametric region around half of the pump frequency in a continuously driven OPO. We also model the OPO dynamics through a single time-domain mean-field equation, identifying previously unknown dynamical regimes, induced by modulation instabilities, which lead to comb formation. Numerical simulation results are in good agreement with experimentally observed spectra. Moreover, the analysis of the coherence properties of the simulated spectra shows the existence of correlated and phase-locked combs. Our results reveal previously unnoticed dynamics of an apparently well assessed optical system, and can lead to a new class of frequency comb sources that may stimulate novel applications by enabling straightforward access to elusive spectral regions, such as the midinfrared.

DOI: [10.1103/PhysRevLett.121.093903](https://doi.org/10.1103/PhysRevLett.121.093903)

Optical frequency comb (OFC) generation in passive nonlinear cavities has attracted increasing interest over the last decade as an alternative approach to the traditional techniques based on femtosecond mode-locked lasers [1,2]. The vast majority of studies have focused on comb formation via third-order $\chi^{(3)}$ nonlinear interactions [3–6]. More recently, however, OFCs have also been demonstrated in continuously driven cavities with quadratic $\chi^{(2)}$ nonlinearities [7–10]. In particular, OFCs can be generated in a cavity with a $\chi^{(2)}$ nonlinear crystal that is phase matched for second harmonic generation (SHG) [9,10]. When the SHG cavity is pumped beyond the threshold for the onset of a so-called internally pumped optical parametric oscillation [11–13], other cascaded $\chi^{(2)}$ processes occur, eventually leading to a comb emission around both the fundamental and second harmonic frequencies.

A particularly attractive feature of quadratic resonators is that they can permit the generation of frequency combs in spectral regions far from the pump frequency. For example, phase-matched SHG can allow for the generation of visible frequency combs by using near-infrared (near-IR) pump

laser. On the other hand, numerical simulations [14] suggest that the inverse process of parametric down-conversion could similarly allow for direct generation of frequency combs in the elusive mid-infrared (mid-IR) region. Conversely, since Kerr microresonators can only generate combs around the pump wavelength, the scarcity of mid-IR continuous-wave (cw) lasers and appropriate nonlinear crystals prevents that technology from being directly applied in the mid-IR region. Applications such as molecular spectroscopy [15,16] would greatly benefit from a technology that allows for more straightforward and efficient generation of mid-IR frequency combs than existing solutions, based on the nonlinear transfer of near-IR OFCs in a separate stage [17–27].

Although the prospect of generating frequency combs through direct intracavity parametric down-conversion is attractive, no experimental demonstration has been reported, so far. The possibility of generating several new frequency components in a singly resonant, non-degenerate OPO was theoretically predicted already in 1969 [28]. Well before the first clear demonstration of degenerate OPO emission [29], several theoretical studies

have been devoted to the description of cw pumped OPOs where both the pump and the degenerate parametric fields resonate [30,31], revealing a rich variety of dynamical regimes. However, these pioneering modeling efforts neglected both diffraction and dispersion. Models that include the effect of diffraction predict the formation of transverse spatial structures, such as roll patterns or solitons [32–37]. The existence of stable pulsed states (solitons or temporal patterns) has meanwhile been predicted by including the effects of group velocity dispersion or spectral filtering in the model equations [38–41]. Of course, the spectral counterpart of such temporal structures would constitute a frequency comb.

Here, we experimentally demonstrate the generation of quadratic frequency combs in a cw pumped, degenerate, doubly resonant OPO. Significantly, we observe comb emission both around the pump angular frequency $2\omega_0$ and in the parametric spectral range around the degeneracy frequency ω_0 . We also present a time domain theoretical model for the intracavity field dynamics that includes the effects of cavity dispersion, and we derive a single mean-field equation that governs the evolution of the slowly varying field amplitude at the parametric frequency. We find that the inclusion of dispersion induces a modulation instability of constant solutions predicted by the usual, dispersionless OPO model [42], and can be responsible for the formation of comb spectral structures.

To model comb dynamics in our OPO system, we consider an optical parametric oscillator pumped by the field B_{in} at $2\omega_0$, which operates near degeneracy, so that signal and idler fields can be described by a single field envelope A . We assume that the cavity of length L is filled with the nonlinear medium, and is resonant only for parametric waves, while the cw pump beam B_{in} leaves the cavity after each round-trip. We also assume that the wave vectors k_1 and k_2 at ω_0 and $2\omega_0$, respectively, satisfy the degenerate phase matching condition $\Delta k = 2k_1 - k_2 = 0$.

OPO dynamics can be described by an infinite dimensional map for the field amplitudes. The map consists of coupled propagation equations that describe the evolution of the field amplitudes at ω_0 and $2\omega_0$ over one cavity round-trip, as well as boundary conditions that describe the input and output relations for the fields at the beginning of each round-trip. Following the approach of Ref. [43], the infinite dimensional map can be combined into a single mean-field equation for the parametric field A [44],

$$\begin{aligned}
 t_R \frac{\partial A(t, \tau)}{\partial t} = & \left(-\alpha_1 - i\delta_1 - i \frac{Lk_1''}{2} \frac{\partial^2}{\partial \tau^2} \right) A \\
 & - \mu^2 A^* [A^2(t, \tau) \otimes I(\tau)] \\
 & + i\mu B_{\text{in}} A^* e^{-i\xi} \text{sinc}(\xi). \quad (1)
 \end{aligned}$$

Here, t is a “slow time” variable that describes the envelope’s evolution over successive round-trips, while

the “fast time” τ describes the temporal profiles of the fields in a reference frame moving with the group velocity of light at ω_0 , α_1 is the total cavity linear losses, $\delta_1 \simeq (\omega_0 - \omega_c)t_R$ is the phase detuning between the parametric field and the closest cavity resonance with frequency ω_c , t_R is the round-trip time, $k_1'' = d^2k/d\omega^2|_{\omega_0}$ is the group velocity dispersion coefficient at ω_0 , $\mu = \kappa L$, where κ is the nonlinear coupling constant, and $\xi = \Delta k L/2$ is the wave vector mismatch parameter. The symbol \otimes denotes the convolution operator and $I(\tau) = \mathcal{F}^{-1}[\hat{I}(\Omega)]$ is a nonlinear response function, where $\hat{I}(\Omega) = (1 - ix - e^{-ix})/x^2$, with $x \equiv x(\Omega) = [\Delta k + i\hat{k}(\Omega)]L$ and $\hat{k}(\Omega) = -\alpha_{c,2}/2 + i[\Delta k'\Omega + (k_2''/2)\Omega^2]$. In the last expressions, the spectral frequency Ω is the offset angular frequency with respect to ω_0 , $\Delta k' = dk/d\omega|_{2\omega_0} - dk/d\omega|_{\omega_0}$ is the group-velocity mismatch, or temporal walk-off, between the fields at ω_0 and $2\omega_0$, $\alpha_{c,2}$ are the propagation losses at $2\omega_0$, and $k_2'' = d^2k/d\omega^2|_{2\omega_0}$ is the group velocity dispersion coefficient at $2\omega_0$.

Equation (1) is a generalization of the dissipative nonlinear Schrödinger equation, with a parametric driving term [39,40] and a noninstantaneous interaction term [45–47]. The function $I(\tau)$ is the same nonlinear response kernel that describes singly resonant cavity SHG [43,48]: physically, it is related to the nonlinear losses and phase shifts due to the cascaded sum frequency generation process. Equation (1) has a trivial zero solution, $A = 0$, and a nontrivial time independent solution, $A_0 = |A_0|e^{i\phi}$. Both the trivial and nonzero solutions can exhibit modulation instability (MI) gain, which reinforces random fluctuations and leads to the exponential growth of sidebands around the carrier frequency ω_0 , and eventually to the formation of frequency combs (Supplemental Material, Sec. 2 [44]). Figure 1 shows the MI gain for the constant finite and zero solutions, respectively, as a function of the offset frequency $\Omega/2\pi$ and the relative detuning $\Delta = \delta_1/\alpha_1$. For positive detunings, both solutions display MI gain, with frequency symmetric

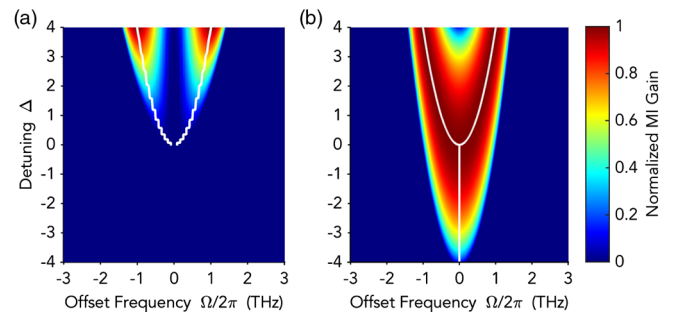


FIG. 1. MI gain of (a) the nonzero constant solution and (b) trivial zero solution, as a function of the offset frequency $\Omega/2\pi$ and the detuning Δ , calculated for our experimental parameters: $\alpha_1 = 0.017$, $L = 15$ mm, $k_1'' = 0.234$ ps²/m, $k_2'' = 0.714$ ps²/m, $\Delta k' = 792$ ps/m, $\kappa = 6.58$ W^{-1/2} m⁻¹, $\xi = 0$, $P_{\text{in}} = 300$ mW. White curves highlight the maxima of the instability gain.

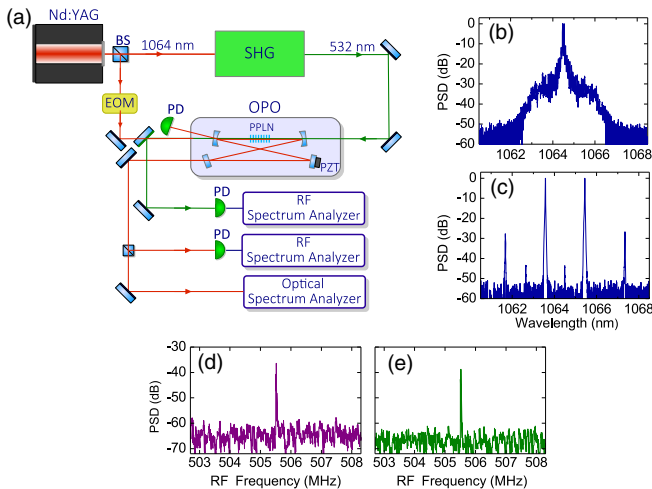


FIG. 2. (a) Schematic of the experimental setup. Beam splitter (BS), electro-optic phase modulator (EOM); piezoelectric actuator (PZT), photodiode (PD). (b) and (c) Experimental infrared comb spectra with zero cavity detuning for different values of the pump power (resolution bandwidth, RBW = 6 GHz). (d) and (e) rf spectra showing beat notes at 505 MHz, in the IR and visible region, respectively, corresponding to the comb spectrum shown in (b) (RBW = 1 kHz).

pairs of gain maxima. For $\Delta > 0$, the critical frequency Ω_{\max} for which the MI gain is maximum (white curves in Fig. 1) nicely follows the relation $\Omega_{\max}^2 = (2/Lk_1')\delta_1$, analogously to the spatial case of transverse pattern formation in different nonlinear optical systems [49–51]. For zero and negative detunings, the zero solution still exhibits MI gain, with peak gain at $\Omega = 0$. It is worth mentioning that, as in SHG systems, the walk-off $\Delta k'$ plays a key role in determining the MI gain profile associated with the nonzero solution. Indeed, for the parameters quoted in Fig. 1, MI only manifests itself for relatively high walk-off values, while it is absent for zero walk-off (Supplemental Material, Fig. S1 [44]). In contrast, the instability of the zero solution, which is not expected in the usual dispersionless analysis of the doubly resonant OPO, does not depend on the walk-off, but is rather induced by group-velocity dispersion. A similar dynamic instability arises in the spatial case, when diffraction is considered [32].

Our experiment is based on a degenerate OPO pumped by a frequency doubled cw Nd:YAG laser [see Fig. 2(a)]. The OPO is based on a temperature-stabilized, 15-mm-long, periodically poled 5%-MgO-doped lithium niobate crystal (PPLN), with a grating period $\Lambda = 6.92 \mu\text{m}$, enclosed in a bow-tie cavity resonating for the parametric wavelengths around 1064 nm (further details are given in the Supplemental Material, Sec. 3 [44]). The cavity has a free spectral range (FSR) of $505 \pm 1 \text{ MHz}$, and a finesse of 180, the linear propagation losses at ω_0 being less than 1% over one round-trip. To make sure that the OPO cavity is resonant at the degeneracy frequency ω_0 , the cavity is

frequency locked by the Pound-Drever-Hall (PDH) technique [52], using the phase modulated IR laser light reflected by a beam splitter, which is injected in the OPO cavity in a direction opposite to the SH pump beam. The PDH error signal is processed by an electronic servo control and fed to the cavity piezoelectric actuator that moves one of the cavity mirrors. The laser, emitting 2 W at 1064 nm (Innolight, Mephisto 2000), is frequency doubled in a periodically poled lithium tantalate (PPLT) crystal placed in an external SHG cavity [53]. We determined the phase-matching temperature for degenerate operation of the OPO to be $T = (61.0 \pm 0.1)^\circ\text{C}$ by maximizing the efficiency of the SHG when pumped directly with the Nd:YAG laser.

The spectral composition of the parametric waves is analyzed by an optical spectrum analyzer (OSA), while two fast photodiodes monitor the light coupled out of the cavity in the respective optical ranges around ω_0 and $2\omega_0$. We note that, because of its limited spectral range (600–1700 nm), our OSA is not capable of detecting the comb around the SH frequency. Rather, evidence of the SH comb is inferred from the radio-frequency (rf) spectrum of the photodiode signal.

The typical power threshold for the onset of degenerate single-frequency OPO emission is around 30 mW. By further increasing the pump power to about 85 mW, we observe the generation of a stable optical frequency comb. Figure 2(b) shows the spectra detected by pumping the OPO with $P_{\text{in}} = 300 \text{ mW}$ of green light, corresponding to an integrated IR power of 120 mW for the signal field at the cavity output. In this case, we detected narrow 1-kHz-resolution-limited beat notes at 1 FSR in the IR and visible, as shown in Figs. 2(d) and 2(e), respectively. This indicates a comb structure with lines equally spaced by one cavity FSR (at least, within the 1 kHz instrumental resolution) both around the pump frequency $2\omega_0$ and the parametric frequency ω_0 . When $P_{\text{in}} = 520 \text{ mW}$, the IR comb emission changes to a few teeth around the degeneracy point, with a spacing of about 500 GHz, as shown in Fig. 2(c). In this case, the absence of beat notes within the bandwidth of the fast detectors suggests that the spectral peaks are indeed isolated single lines. As the pump power further increases, the stability of the OPO cavity locking deteriorates, and the error signal starts to oscillate erratically, thus precluding the observation of stable comb emission.

We also experimentally studied the effect of the cavity detuning on the comb spectra. To this end, we added a voltage offset to the error signal used for cavity locking, which allowed us to explore relative phase detunings Δ between -0.3 and 0.3 . Figures 3(a)–3(c) show the experimental comb spectra recorded for $\Delta = -0.30, 0.00, +0.30 (\pm 0.02)$, respectively, for 300 mW of pump power. Corresponding spectra obtained from numerical simulations are shown in Figs. 3(d)–3(f). Experimental spectra for negative and zero detunings are very similar, displaying a

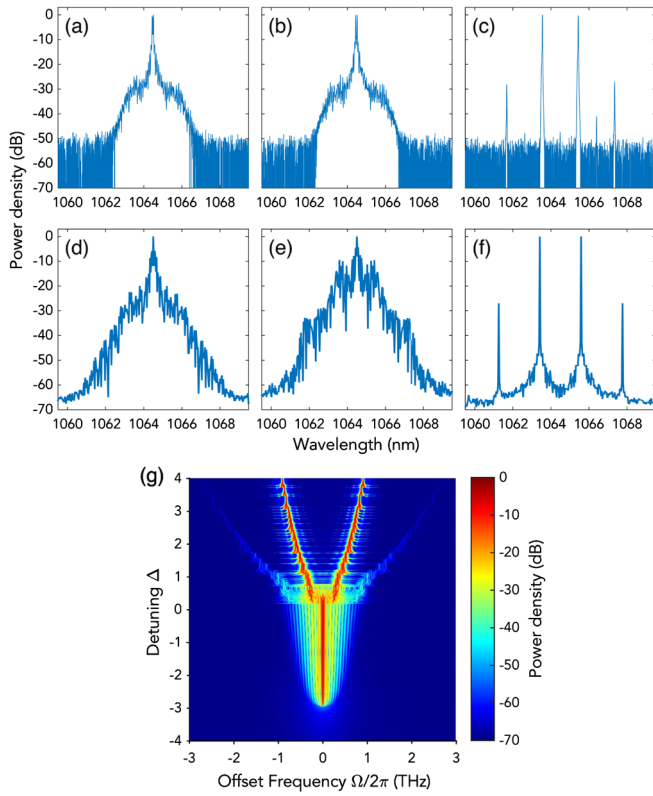


FIG. 3. Normalized infrared OPO spectra for different cavity detunings. (a)–(c) experimental spectra for relative detunings $\Delta = -0.3, 0, +0.3$, respectively. (d)–(f) corresponding numerically calculated spectra. (g) Map of calculated OPO spectra as a function of the offset from the degeneracy frequency and the relative detuning. Measurements and simulations refer to 300 mW of pump power.

1 FSR line spacing, while, for the positive detuning, the experimental spectrum consists of two pairs of symmetric lines, very similar to that observed in Fig. 2(c). We found a good agreement with the corresponding spectra, shown in Figs. 3(d)–3(f), calculated by numerically integrating Eq. (1) over the slow time t (Supplemental Material, Sec. 1 [44]). All the simulation parameters are listed in the caption of Fig. 1. Numerical simulations show that the spectrum of Fig. 2(c) is still a possible solution of the model of Eq. (1), but for a different set of parameters. We believe, however, that the discrepancy can hardly be ascribed to imprecise knowledge of the parameters alone. Rather, we speculate that additional effects, such as thermo-optical nonlinearities, might underlie the observed discordance, as well as the instability of the cavity locking at high pump power.

To give a more comprehensive picture of the comb dynamics, we simulated the evolution of the comb spectrum as function of Δ over a wider range of values than those accessible in our experiments. In this case, we swept the detuning from negative to positive values over 10^7 round-trips. As shown in Fig. 3(g), for negative and small

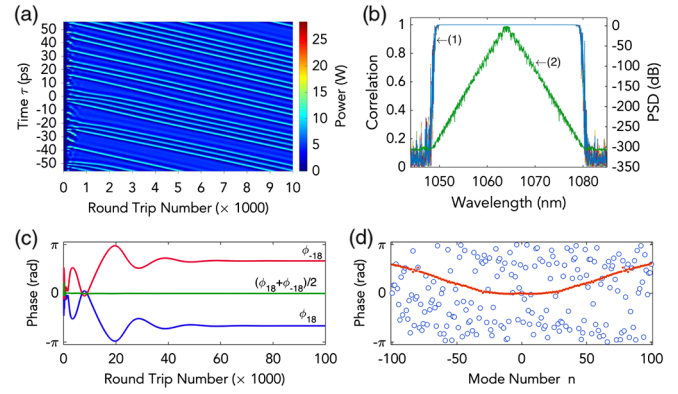


FIG. 4. Coherence analysis. (a) Temporal evolution of the parametric field envelope ($t_R = 111$ ps, $P_{in} = 300$ mW, and $\Delta = -2$). (b) Traces (1) are the first order correlation function $g^{(1)}(m, \lambda)$ as a function of wavelength, calculated for different time delays up to $100 \mu\text{s}$; trace (2) is the comb spectrum profile. (c) Offset phase evolution for two symmetric modes ± 18 and their average phase. (d) Steady state offset phase (blue open circles) and symmetric average phase (red dots), as a function of mode number n .

positive detunings, we observe comb spectra with 1-FSR-spaced lines. Around $\Delta = 0.3$ the spectra show a sharp transition to a different power distribution, but still with a 1 FSR mode spacing, which, as the detuning further increases ($\Delta \gtrsim 1$), evolves into small 1-FSR-spaced lines groups, which are widely spaced from the degeneracy frequency. In general, the spectral dynamics is in good agreement with the expected MI gain. Finally, we notice that, while dispersion is essential for comb formation, it also entails a frequency dependent cavity FSR, which eventually sets a limit on the spectral bandwidth of the resulting combs, as we numerically checked (Supplemental Material, Fig. S2 [44]).

Numerical simulations also provide insights into the time-domain emission profile, which cannot be experimentally accessed due to the insufficient bandwidth of our photodetectors. Simulations of quadratic combs in cavity SHG have shown stable steady state solutions with repeatable and regular temporal patterns, such as Turing patterns or solitary waves, which exhibit phase locking [43,48,54,55]. Interestingly, simulations of our OPO show that, in general, the intracavity temporal profiles do not correspond to regular patterns, and that their precise form depends sensitively on the random seed used as initial condition. Nevertheless, even though the temporal profiles do not correspond to clean pulse trains, the frequency combs can still exhibit a high degree of coherence for a wide range of pump powers and detunings. Figure 4(a) shows the time evolution of the parametric field envelope over the first 10,000 round-trips ($\sim 1 \mu\text{s}$). The field profile rapidly evolves to a steady state, slowly drifting in the frame of reference that moves at the group velocity of the light at ω_0 . As in SHG combs [43,48,54], the relative drift of the temporal pattern, much slower than the walk-off $\Delta k'$,

indicates a nonlinear compensation of the walk-off induced linear spectral phase, which can lead, in principle, to group-velocity-locked fundamental and parametric waves.

To quantify the coherence of this state, we calculated the first-degree correlation function [56] $g^{(1)}(m, \lambda) = |\langle \tilde{E}^*(t_j, \lambda) \tilde{E}(t_{j+m}, \lambda) \rangle| / \langle |\tilde{E}(t_j, \lambda)|^2 \rangle$, where $\tilde{E}(t_j, \lambda)$ is the Fourier transform of the complex intracavity field, calculated at multiples of the round-trip time $t_j = jt_R$, with j an integer number. Angle brackets denote an ensemble average. As shown in Fig. 4(b), after reaching steady state, we obtained an almost perfect correlation $g^{(1)}(m, \lambda) = 1$, over a 100 μs time scale ($m \simeq 10^6$), for all the comb teeth that emerge from the noise floor. For each comb mode n , we calculated the phase φ_n as a function of the round-trip time. Figure 4(c) shows the evolution of the relative phase $\phi_n = \varphi_n - \varphi_0$ for two symmetric modes, $n = \pm 18$. We notice that, on the time scale of several tens of thousands of t_R , each phase settles to a steady value, which randomly depends on the initial seeding noise [open circles, Fig. 4(d)]. Nevertheless, the average phase of pairs of symmetric modes, e.g., $(\phi_{18} + \phi_{-18})/2$, settles to a steady value on a shorter time scale (a few times the cavity photon lifetime), and exhibits a regular and reproducible trend, when we repeat the same simulation with a different seeding random noise, as shown by the seemingly smooth distribution of red dots in Fig. 4(d). The rapid antisymmetrization of the phase profile around the degeneracy frequency is essentially related to the intrinsic symmetry of the process that initiates the comb (modulation instability, in our case), and can eventually lead to comb mode phase locking [57]. It is noteworthy that an indirect experimental evidence of this intermodal phase coherence is provided by the narrow resolution-limited beat notes shown in Figs. 2(d) and 2(e).

In conclusion, we have experimentally demonstrated frequency comb generation in a cw pumped degenerate OPO, and theoretically derived a mean-field equation, which rather well describes the observed dynamical regimes. Our findings disclose new aspects of OPO dynamics, never observed till now, and open an entirely new scenario in the field of nonlinear optics. In fact, our theoretical framework can be extended to other OPO configurations, such as nondegenerate and triply resonant OPOs. In view of the increasing number of applications of OFCs in many fields of physics, our work paves the route to a new class of devices, which could efficiently provide OFCs in spectral regions, such as the mid-IR, where comb sources are highly desirable but still difficult to get. Exploiting the described comb generation scheme, a larger comb bandwidth could be enabled by tailoring the dispersion in chip-scale waveguide resonators that exhibit large intrinsic or induced second-order nonlinearity, through efficient quasiphase matching schemes [58,59].

The authors acknowledge financial support by the Ministero dell'Istruzione, dell'Università e della Ricerca

(Projects PRIN-2015KEZNYM “NEMO–Nonlinear dynamics of optical frequency combs” and FIRB n. RBF13QUV1 “Optomechanical tailoring of squeezed light”); Ministero degli Affari Esteri e della Cooperazione Internazionale (Project “NOICE Joint Laboratory”); and Rutherford Discovery Fellowships and Marsden fund of the Royal Society of New Zealand. The research leading to these results has received funding from the European Union’s Horizon 2020 research and innovation programme under the Marie Skłodowska-Curie grant agreement No. GA-2015-713694. The work of S. W. is supported by the Ministry of Education and Science of the Russian Federation (Minobrnauka) (14.Y26.31.0017).

*simona.mosca@ino.it

†maurizio.derosa@ino.it

- [1] R. Holzwarth, T. Udem, T. W. Hänsch, J. C. Knight, W. J. Wadsworth, and P. S. J. Russell, *Phys. Rev. Lett.* **85**, 2264 (2000).
- [2] D. J. Jones, S. A. Diddams, J. K. Ranka, A. J. Stentz, R. S. Windeler, J. L. Hall, and S. T. Cundiff, *Science* **288**, 635 (2000).
- [3] P. Del’Haye, A. Schliesser, O. Arcizet, T. Wilken, R. Holzwarth, and T. J. Kippenberg, *Nature (London)* **450**, 1214 (2007).
- [4] Y. K. Chembo, D. V. Strekalov, and N. Yu, *Phys. Rev. Lett.* **104**, 103902 (2010).
- [5] T. Hansson, D. Modotto, and S. Wabnitz, *Phys. Rev. A* **88**, 023819 (2013).
- [6] T. J. Kippenberg, R. Holzwarth, and S. A. Diddams, *Science* **332**, 555 (2011).
- [7] V. Ulvila, C. R. Phillips, L. L. Halonen, and M. Vainio, *Opt. Lett.* **38**, 4281 (2013).
- [8] V. Ulvila, C. R. Phillips, L. L. Halonen, and M. Vainio, *Opt. Express* **22**, 10535 (2014).
- [9] I. Ricciardi, S. Mosca, M. Parisi, P. Maddaloni, L. Santamaria, P. De Natale, and M. De Rosa, *Phys. Rev. A* **91**, 063839 (2015).
- [10] S. Mosca, I. Ricciardi, M. Parisi, P. Maddaloni, L. Santamaria, P. De Natale, and M. De Rosa, *Nanophotonics* **5**, 316 (2016).
- [11] S. Schiller, G. Breitenbach, R. R. Paschotta, and J. Mlynek, *Appl. Phys. Lett.* **68**, 3374 (1996).
- [12] S. Schiller, R. Bruckmeier, and A. G. White, *Opt. Commun.* **138**, 158 (1997).
- [13] A. G. White, P. K. Lam, M. S. Taubman, M. A. M. Marte, S. Schiller, D. E. McClelland, and H.-A. Bachor, *Phys. Rev. A* **55**, 4511 (1997).
- [14] T. Hansson, F. Leo, M. Erkintalo, J. Anthony, S. Coen, I. Ricciardi, M. De Rosa, and S. Wabnitz, *J. Opt. Soc. Am. B* **33**, 1207 (2016).
- [15] A. Schliesser, N. Picqué, and T. W. Hänsch, *Nat. Photonics* **6**, 440 (2012).
- [16] P. Maddaloni, P. Cancio Pastor, and P. De Natale, *Meas. Sci. Technol.* **20**, 052001 (2009).
- [17] P. Maddaloni, P. Malara, G. Gagliardi, and P. De Natale, *New J. Phys.* **8**, 262 (2006).

- [18] C. Erny, K. Moutzouris, J. Biegert, D. Kühlke, F. Adler, A. Leitenstorfer, and U. Keller, *Opt. Lett.* **32**, 1138 (2007).
- [19] J. H. Sun, B. J. S. Gale, and D. T. Reid, *Opt. Lett.* **32**, 1414 (2007).
- [20] F. Adler, K. C. Cossel, M. J. Thorpe, I. Hartl, M. E. Fermann, and J. Ye, *Opt. Lett.* **34**, 1330 (2009).
- [21] S. T. Wong, K. L. Vodopyanov, and R. L. Byer, *J. Opt. Soc. Am. B* **27**, 876 (2010).
- [22] N. C. Leindecker, A. Marandi, R. L. Byer, and K. L. Vodopyanov, *Opt. Express* **19**, 6296 (2011).
- [23] N. N. Leindecker, A. A. Marandi, R. L. R. Byer, K. L. Vodopyanov, J. J. Jiang, I. I. Hartl, M. M. Fermann, and P. G. P. Schunemann, *Opt. Express* **20**, 7046 (2012).
- [24] F. Keilmann and S. Amarie, *J. Infrared Millimeter Terahertz Waves* **33**, 479 (2012).
- [25] I. Galli, F. Cappelli, P. Cancio, G. Giusfredi, D. Mazzotti, S. Bartalini, and P. De Natale, *Opt. Express* **21**, 28877 (2013).
- [26] A. Gambetta, N. Coluccelli, M. Cassinerio, D. Gatti, P. Laporta, G. Galzerano, and M. Marangoni, *Opt. Lett.* **38**, 1155 (2013).
- [27] Q. Ru, Z. E. Loparo, X. Zhang, S. Crystal, S. Vasu, P. G. Schunemann, and K. L. Vodopyanov, *Opt. Lett.* **42**, 4756 (2017).
- [28] L. B. Kreuzer, *Proceedings of the Joint Conference on Lasers and Opto-Electronics* (I.E.R.E., London, 1969), p. 52.
- [29] C. D. Nabors, S. T. Yang, T. Day, and R. L. Byer, *J. Opt. Soc. Am. B* **7**, 815 (1990).
- [30] P. D. Drummond, K. J. McNeil, and D. F. Walls, *Opt. Acta* **27**, 321 (1980).
- [31] L. A. Lugiato, C. Oldano, C. Fabre, E. Giacobino, and R. J. Horowicz, *Il Nuovo Cimento D* **10**, 959 (1988).
- [32] G.-L. Oppo, M. Brambilla, and L. A. Lugiato, *Phys. Rev. A* **49**, 2028 (1994).
- [33] G.-L. Oppo, M. Brambilla, D. Camesasca, A. Gatti, and L. A. Lugiato, *J. Mod. Opt.* **41**, 1151 (1994).
- [34] G. J. de Valcárcel, K. Staliunas, E. Roldán, and V. J. Sanchez-Morcillo, *Phys. Rev. A* **54**, 1609 (1996).
- [35] K. Staliunas, *J. Mod. Opt.* **42**, 1261 (1995).
- [36] S. Longhi, *Phys. Rev. A* **53**, 4488 (1996).
- [37] S. Longhi, *Phys. Scr.* **56**, 611 (1997).
- [38] S. Longhi, *Opt. Lett.* **20**, 695 (1995).
- [39] S. Longhi, *Opt. Lett.* **21**, 860 (1996).
- [40] S. Longhi, *J. Mod. Opt.* **43**, 1089 (1996).
- [41] S. Longhi, *Phys. Rev. E* **53**, 5520 (1996).
- [42] R. W. Boyd, *Nonlinear Optics*, 3rd ed. (Academic Press, Burlington, 2008).
- [43] F. Leo, T. Hansson, I. Ricciardi, M. De Rosa, S. Coen, S. Wabnitz, and M. Erkintalo, *Phys. Rev. Lett.* **116**, 033901 (2016).
- [44] See Supplemental Material at <http://link.aps.org/supplemental/10.1103/PhysRevLett.121.093903> for the detailed derivation and the stability analysis.
- [45] B. Kibler, C. Michel, J. Garnier, and A. Picozzi, *Opt. Lett.* **37**, 2472 (2012).
- [46] T. Hansson, D. Modotto, and S. Wabnitz, *Opt. Lett.* **39**, 6747 (2014).
- [47] Y. Okawachi, M. Yu, V. Venkataraman, P. M. Latawiec, A. G. Griffith, M. Lipson, M. Lončar, and A. L. Gaeta, *Opt. Lett.* **42**, 2786 (2017).
- [48] T. Hansson, F. Leo, M. Erkintalo, S. Coen, I. Ricciardi, M. De Rosa, and S. Wabnitz, *Phys. Rev. A* **95**, 013805 (2017).
- [49] K. Staliunas and V. J. Sanchez-Morcillo, *Opt. Commun.* **177**, 389 (2000).
- [50] U. Bortolozzo, P. Villoresi, and P. L. Ramazza, *Phys. Rev. Lett.* **87**, 274102 (2001).
- [51] A. Esteban-Martín, J. García, E. Roldán, V. B. Taranenko, G. J. de Valcárcel, and C. O. Weiss, *Phys. Rev. A* **69**, 033816 (2004).
- [52] R. W. P. Drever, J. L. Hall, F. V. Kowalski, J. Hough, G. M. Ford, A. J. Munley, and H. Ward, *Appl. Phys. B* **31**, 97 (1983).
- [53] I. Ricciardi, M. De Rosa, A. Rocco, P. Ferraro, and P. De Natale, *Opt. Express* **18**, 10985 (2010).
- [54] F. Leo, T. Hansson, I. Ricciardi, M. De Rosa, S. Coen, S. Wabnitz, and M. Erkintalo, *Phys. Rev. A* **93**, 043831 (2016).
- [55] M. Parisi, N. Morais, I. Ricciardi, S. Mosca, T. Hansson, S. Wabnitz, G. Leo, and M. De Rosa, *J. Opt. Soc. Am. B* **34**, 1842 (2017).
- [56] M. Erkintalo and S. Coen, *Opt. Lett.* **39**, 283 (2014).
- [57] Y. H. Wen, M. R. E. Lamont, S. H. Strogatz, and A. L. Gaeta, *Phys. Rev. A* **94**, 063843 (2016).
- [58] N. Morais, I. Roland, M. Ravaro, W. Hease, A. Lemaître, C. Gomez, S. Wabnitz, M. De Rosa, I. Favero, and G. Leo, *Opt. Lett.* **42**, 4287 (2017).
- [59] E. Timurdogan, C. V. Poulton, M. J. Byrd, and M. R. Watts, *Nat. Photonics* **11**, 200 (2017).